A Simplified Reaction Mechanism for Soot Formation in Nonpremixed Flames

K. M. LEUNG, and R. P. LINDSTEDT
Fluids Section, Department of Mechanical Engineering, Imperial College, London SW7 2BX

and

W. P. JONES
Department of Chemical Engineering and Chemical Technology, Imperial College, London SW7 2BY

The present article outlines a simplified reaction mechanism for the formation, growth, and combustion of soot particles in laminar nonpremixed flames. The model can be combined with detailed chemistry descriptions for the gas phase, as in the present case, or with reduced chemical reaction mechanisms. The reaction mechanism involves nucleation, surface growth, particle coagulation, and combustion steps. The model outlined has been created with the intention of being applicable to the prediction of turbulent flames via different approaches. The soot nucleation and surface growth reactions are linked to the gas phase by presuming that pyrolysis products, in the present case acetylene, and not the fuel itself, are of primary importance in the soot formation process. The deduced reaction mechanism is applied to counterflow ethylene and propane flames burning with a range of oxygen-enriched and -depleted air streams. The results obtained show excellent qualitative and quantitative agreement with measured data for soot volume fraction, particle growth, and number density.

INTRODUCTION

The problem posed by the accurate prediction of soot formation in laminar and turbulent combustion is formidable. It is also of great practical importance, particularly in nonpremixed combustion applications ranging from turbulent jet flames to internal combustion engines and gas turbine combustion chambers. At the present time detailed soot formation models have been suggested [1] and progress made [2], although these models must still be regarded as being far from complete because qualitative understanding of the physical processes remains uncertain. The complexity of these models will also inevitably preclude their use in flows of practical importance for many years to come. Regarding global soot models, many have been proposed, as discussed below. However, their applicability is questionable under conditions different from those under which they were originally formulated. The latter point is particularly relevant with reference to practical applications that frequently operate under conditions where experimental data are difficult or impossible to obtain. Consequently there is currently a significant need for accurate and reliable simplified descriptions. Although most practical applications are strongly turbulent in nature a most basic requirement of any model is the successful prediction of soot characteristics under a wide range of laminar conditions. Unfortunately, even the latter problem is one of great complexity in particular as any deduced reaction mechanism must be sufficiently compact to be implemented into turbulent flame predictions for example via an extended laminar flamelet presumed *pdf* approach [3] or via a transported *pdf* approach [4].

Simplified models have in the past been proposed by Tesner et al. [5], Gilyazefdinov [6], and Kennedy et al. [7]. The former of these has been applied by Magnussen [8] in the prediction of turbulent flames, although it was found necessary to vary the rate constants by more than an order of magnitude from those suggested for laminar flames. The model of Gilyazefdinov has been calibrated using the experimental data of Moss et al. [9] and applied to laminar [9] and turbulent flames [10] with improved agreement. However, both of these models have a very simple description of the gas-phase chemistry-soot interaction

0010-2180/91/$3.50

whereby the formation of soot is linked directly to the fuel concentration. Nevertheless, the approach of Moss et al. [9] has been found to work well for conditions close to those where the model was calibrated. The present generation of optical measurement techniques are also not well suited for use in the heavily sooting conditions that arise in many practical configurations, and the application of the model to such conditions may consequently prove difficult. However, progress is being made also in the area of more highly sooting flames [11].

From past experimental and theoretical work it can be noted that there is fairly broad agreement [2, 12] on the basic steps required to model the formation and emissions of soot particulates within the framework of simplified models. These steps include soot nucleation, surface growth, particle coagulations, and finally destruction via combustion. The current models, outlined above, suffer from the rather obvious shortcoming that the soot formation process is linked directly to the parent fuel concentrations, an aspect that is not in agreement with experimental data. Rather, measurements indicate that soot formation is dependent upon the breakdown path of the fuel and the presence of pyrolysis products such as acetylene and polyunsaturated cyclical hydrocarbons such as benzene.

In view of the above a different approach is adopted in the present work whereby it is assumed that the presence of pyrolysis products is a crucial feature of the soot formation process. Here acetylene (C_2H_2) is used as the indicative critical specie in the soot formation process. The choice of acetylene is strongly supported by experimental evidence, for example, Harris and Weiner [13, 14]. However, as pyrolysis products tend to show similar profiles with different magnitudes in a flame the currently proposed model would work also with other critical species provided a factor of proportionality is introduced. This is supported by the measurements of Smyth et al. [15] which indicate that other species commonly associated with soot formation, such as C_6H_6, C_4H_2, and C_4H_6, all show profiles of similar shape but with varying magnitudes. However, it should be noted that the downstream evolution of the C_6H_6 profile differs from that of C_2H_2 [15] in the co-flowing geometry. It can consequently not be ruled out that C_6H_6 concentrations may prove a superior choice as an indicative specie, particularly for incipient particle formation. However, the important feature of the present model is that the sooting propensity of a particular fuel-oxidant system is linked quantitatively to the regions of the flame where gas-phase pyrolysis occurs.

A significant aid in the quantitative formulation of simplified models is the progress made by the use of laser extinction methods in measurements in both laminar [15–18] and turbulent [19, 20] flames with low to moderate soot yields. A number of experimental studies of soot formation in laminar flames have been performed that lend support to the approach adopted in the present study, in particular those by Vandsburger et al. [21], Harris and Weiner [13, 14], Kent and Wagner [16], and Kent and Honnery [18]. In the present study the counterflow flames measured by Vandsburger et al. [21] have been utilized extensively, as they represent a consistent set of data on soot volume fraction, particle size, and number density under greatly varying conditions. In view of the planned future application to the turbulent case attention is focused primarily on ethylene (C_2H_4) flames—most of the experimental data on soot formation in turbulent flames has been obtained using this fuel. However, predictions for propane (C_3H_8) are also reported to emphasize the generality of the model.

Of particular relevance to the formulation of the current model is a qualitatively, and as far as possible, quantitatively, correct description of the gas-phase kinetics. This is a difficult task, as many recent studies have shown [2, 23, 24], and there remains considerable uncertainty in the quantitative prediction of levels of radical species such as CH in rich acetylene flames and major species such as C_3H_6 along with C_3 radicals in propane flames. However, there is little doubt that the gross features, including C_2H_2 levels, are well predicted qualitatively and in most cases quantitatively, as is shown below.

The preference for the use of detailed gas-phase kinetics in the present study is simply to minimize any additional uncertainties that may be introduced via a systematic reduction. In contrast to alkane fuels [25–27], global (reduced) reaction mechanisms for unsaturated C_2 hydrocarbons and fuel pyrolysis have currently not been sufficiently developed to allow reliable predictions, although

such work is in progress [28]. The gas-phase reaction mechanism used in the current work is based on that formulated by Warnatz and co-workers [29–32], with reaction rates updated according to the recommendations by the CEC Kinetic Data Evaluation Group [33] and recent work by Peters et al. [24]. A few additional reaction steps resulting from the work of Cernansky et al. [34] and Dagaut et al. [35] have also been included. Full details and comparisons with experimental data as available are given below.

SOOT FORMATION MECHANISM

Many modeling approaches are possible in the formulation of a soot formation/destruction mechanism, as outlined above. In the present work the approach taken has been to develop global reaction steps based on the current qualitative understanding of the soot formation process. Furthermore, it has been viewed as essential to minimize the number of independent scalars and to obtain complete information about the reaction steps to facilitate the implementation of the model into turbulent combustion models.

The proposed soot formation mechanism is based on the observation that the presence of pyrolysis intermediates, in particular acetylene, is indicative of the propensity of soot to form [12]. The model involves the solution of two additional conservation equations for soot mass fraction and soot number density. Once a particular particle shape, in the present case assumed to be spherical, is introduced the model is complete.

The soot (mass) formation has been split into two components. The first of these concern the formation of incipient particles. It is well known [12] that soot formation is accompanied by the presence of (poly-)acetylenes and (poly-)aromatic ring systems. Smyth et al. [15] have produced detailed measurements of incipient soot formation in co-flowing methane–air flames that clearly show that initial formation occurs in a region where intermediate hydrocarbons are abundant. The initial soot particles, be they liquid or not, display very rapid mass growth via radical and/or ion reactions. This part of the soot formation process is poorly understood, although there is some evidence that acetylene plays a part in the very rapid initial growth phase [17]. Shock tube studies of hydrocarbon mixtures have indicated that the effective activation temperature (E/R) associated with the early formation process is somewhat lower than that commonly associated with fuel pyrolysis and values in the range 15,000–25,000 K have been reported for different pressures [12]. In the present study it is assumed that active nuclei are formed from pyrolysis products resulting from the breakdown of the fuel. It has further been assumed that the indicative species for this process is acetylene. As has been outlined above, this assumption is acceptable as a first approximation to the location in the flame structure where nuclei are formed. Thus this step is in the present work written as

$$C_2H_2 \rightarrow 2C(s) + H_2. \qquad (1)$$

This reaction step is similar to that outlined by Tesner et al. [5] for premixed acetylene–air flames, although in the present case acetylene is *not* the actual fuel but assumed to be a characteristic product of the fuel breakdown process. The notation $C(s)$ is strictly speaking not correct, as particularly young soot contains significant amount of hydrogen. It has, however, been adopted in the absence of a generally accepted alternative.

To determine a suitable reaction rate constant for the soot nucleation step poses difficulties. Firstly, it must accurately describe the comparatively high activation energy process associated with the formation of incipient soot particles. Secondly, available measurements indicate that the reactivity of the initial surface formed on the incipient particles is significantly more reactive than that of older particles, even if the adsorbed species remains the same. Vandsburger et al. [21] indicates in excess of an order of magnitude higher specific reactivity per unit surface area for fresh particles. To address this problem within the frame work of the soot surface growth step alone is awkward, as it would imply a temporal dependence of the rate constant. Further equations describing the aging of soot particles or the depletion of active adsorption sites can naturally be introduced. However, this adds complexity and uncertainty to the model and consequently a different approach has been adopted at present. This amounts, firstly, to assuming that the initial formation of soot particles is dominated by the

formation of incipient particles *and* initial surface growth and, secondly, to introduce a simple measure to account for particle age in the surface growth process. The latter approximation is discussed below. The former is not too serious, as only a small fraction of the actual soot mass is formed during this stage. Furthermore, measurements indicate [17] that initial surface growth may in any case relate to the local acetylene concentration. The model is thus formulated to reflect the experimental observation [16] that typically less than 10% of the total soot mass is formed by incipient particle formation. However, it should here be emphasized that the reaction step itself is of crucial importance as it determines the initial surface area (or active sites) available for growth and the initial soot number density. The reaction step is at present approximated by assuming that particles are formed with a minimum particle size. It has been assumed that this size corresponds to 100 carbon atoms, giving a particle size of around 1.24 nm. Other choices are naturally possible, but it can be shown that the final results are not strongly dependent on the presumed size of the incipient particle provided this remains in the range 1–10 nm. For the nucleation step Tesner et al. [5] have suggested an activation temperature (E/R) of around 75,500 K, whereas Gilyazefdinov [6] assigned a value of 49,000 K. Computations with these values indicate that the temperature dependence is appreciably exaggerated in the former case and appears still too high for the latter. The most appropriate value to describe both the formation of incipient particles and initial surface growth was found to be around 21,100 K. This value is roughly twice that describing the pure surface growth on older particles, see below, and rather interestingly is in the middle of the range obtained for soot particle formation using shock tube studies [12]. It is also close to the overall activation energy given for the soot formation process by Vandsburger et al. [21]. Thus the nucleation rate constant may in the present case be written as,

$$R_1 = k_1(T)\,[C_2H_2]\,[\mathrm{kmol/m^3/s}],$$

$$k_1(T) = 0.1\,10^5\,e^{-21{,}100/T}\,[1/\mathrm{s}].$$

The preexponential factor was determined from the computation of C_2H_4 flame burning with an oxidant stream consisting of 22% O_2 and 78% N_2 (oxygen index 0.22) and comparisons with measurements.

The second reaction responsible for soot mass formation is assumed to be surface growth due to the adsorption of C_2H_2 on the surface of the particles. This reaction step can be written schematically as

$$C_2H_2 + nC(s) \rightarrow (n+2)C(s) + H_2. \qquad (2)$$

Harris and Weiner [14] have suggested, based on extensive measurements, that the soot mass growth is to a first approximation first order in acetylene concentration. Adopting this suggestion in the modeling of the surface growth step gives a reaction rate source term as,

$$R_2 = k_2(T)f(S)[C_2H_2],$$

where molar concentrations, for example, $[C_2H_2]$, are in units of kmol/m^3-mixture. S is the surface area of soot in m^2/m^3-mixture and $f(S)$ is defined below. The surface area may be written as

$$S = \pi(d_p^2)(\rho N) = \pi\left(\frac{6}{\pi}\frac{1}{\rho_{C(s)}}\frac{Y_{C(s)}}{N}\right)^{2/3}(\rho N)$$

and the particle diameter as

$$d_p = \left(\frac{6}{\pi}\frac{1}{\rho_{C(s)}}\frac{Y_{C(s)}}{N}\right)^{1/3}.$$

It can readily be shown by sample computations that assuming surface growth to have a linear dependence on surface area does not account accurately for changes in conditions throughout the flame. The result of such an approximation is an appreciable exaggeration of the influence of surface area on the soot formation process. This finding is in agreement with recent studies [2, 45] of premixed flames. Thus it remains necessary to account in some approximate way for the reduced reactivity of soot particles due to the effect of aging throughout the flame. In the present work the simple assumption has been made that the number of active sites present locally in the flame is proportional to the square root of the total surface area available locally in the flame. This reduces the dependence on surface area

sufficiently and gives rise to the following rate expression.

$$R_2 = k_2(T)[C_2H_2]\sqrt{\pi\left(\frac{6M_{C(s)}}{\pi\rho_{C(s)}}\right)^{2/3}} \times [C(s)]^{1/3}[\rho N]^{1/6}\,[\text{kmol/m}^3/\text{s}],$$

where $[C(s)]$ is $[\rho Y_{C(s)}/M_{C(s)}]$, N [particles/kg-mixture], Y_k the mass fraction of species k, and M its molar mass in kg/kmol, for example, $M_{C(s)} = 12.011$.

It remains to determine the rate constant $k_2(T)$. For the activation energy directly relevant measurements have been performed by Vandsburger et al. [21], who determined a value of activation temperature (E/R) of around 12,100 K. A large number of computations have been performed using this value during the course of the present work (see below), and the value has been found to describe the temperature dependence of surface growth step sufficiently well. Regarding the pre-exponential factor this was determined by the solution of the complete equation set for the same flame used in the determination of the constant for the nucleation step, for example, a C_2H_4 flame with an oxygen index of 0.22. A value of $0.6*10^4$ was determined, giving the final rate constant for this step as

$$k_2(T) = 0.6*10^4\, e^{-12{,}100/T}[\text{m}^{3/2}/\text{m-soot/s}].$$

The soot oxidation step used in the present work is based on that formulated by Lee et al. [36]. This choice was made because it has been shown [37] to adequately describe the soot burnout in co-flowing C_2H_4-air flames. However, there are currently considerable uncertainties in constructing a more detailed description of soot oxidation [39, 40]. The rate constant was adjusted to conform with the maximum observed specific surface oxidation rate in laminar co-flowing methane-air flames by Garo et al. [40]. It has been assumed that solid carbon is oxidized to form carbon monoxide exclusively at typical flame temperatures.

$$C(s) + 1/2\,O_2 \rightarrow CO. \qquad (3)$$

It should also be noted that in the counterflow geometry soot oxidation occurs only in a very narrow region close to the flame front. Consequently, it can be readily shown that predictions are comparatively insensitive to this reaction step. This latter observation is an advantageous feature of the counterflow geometry because it enables a step-by-step approach to the formulation of a global reaction mechanism. Consequently, the soot oxidation is described with sufficient accuracy for the present purposes by the following reaction step where the dependence on local surface area (S) has been retained.

$$R_3 = k_3(T)S[O_2] \qquad [\text{kmol/m}^3/\text{s}],$$

$$k_3(T) = 0.1*10^5 T^{1/2} e^{-19{,}680/T} \times [\text{m}^3/\text{m}^2\text{-soot/s}].$$

The value of this rate constant is around eight times larger than the value recommended by Lee, Thring and Beer [36] but in agreement with the evaluation by Garo et al. [40] who also argue strongly for the inclusion of the OH radical as an oxidizer. Their results also indicate that the Strickland—Constable [38] reaction rate significantly underestimates the soot oxidation rate. An oxidation step involving the OH radical could readily have been formulated in the context of the present model and considerable support exists for its inclusion, for example, Neoh et al. [46] and Roth et al. [47]. However, the above reaction step is considered sufficiently accurate for the current purposes.

The soot nucleation step outlined above also gives rise to a source term in the number density equation. The decrease in particle number density is simply assumed to occur according to particle agglomeration. This step is modeled using the normal square dependence used by many other investigators, for example, [12],

$$nC(s) \rightarrow C_n(s) \qquad (4)$$

$$R_4 = -2C_a d_p^{1/2}\left(\frac{6\kappa T}{\rho_{C(s)}}\right)(\rho N)^2.$$

Thus the complete source term may be written as

$$R_4 = \frac{2}{C_{\min}} N_A R_1 - k_4(T)[C(s)]^{1/6}[\rho N]^{11/6},$$

$$k_4(T) = 2C_a\left(\frac{6M_{C(s)}}{\pi\rho_{C(s)}}\right)^{1/6}\left(\frac{6\kappa T}{\rho_{C(s)}}\right)^{1/2}.$$

In the above rate expression, N_A is Avogadro's

number (6.022×10^{26} particles/kmol), C_{min} is the number of carbon atoms in the incipient carbon particle (100), κ is the Boltzmann constant (1.38×10^{-23} J/K), $\rho_{C(s)}$ is the soot density (2000 kg/m^3), and C_a is the agglomeration rate constant, assigned a value of 9.0. This value is higher than used by other investigators [16], who have used the value of 3.

The four reaction rates outlined above closes the system for soot mass formation/destruction and particle number density. A consequence of the above formulation is that soot oxidation results in a reduction in the soot mass fraction and the particle diameter, but does not affect the particle number density equation directly. In reality this simple description is naturally questionable. It is, however, considered sufficiently accurate for the present state of model development as the above rate expressions are not strong functions of the particle number density. It should also be noted that other investigators have frequently assumed a constant particle diameter [7, 9], so that the present treatment does provide an improved description in this respect.

GAS-PHASE REACTION MECHANISM

To reduce uncertainties relating to the gas-phase oxidation mechanism a detailed reaction mechanism was implemented in the present study. The reaction mechanism is based on that formulated by Warnatz [29], including subsequent modifications [24, 30, 31, 32] and reaction rates that have been further updated according to the recommendations by the CEC Kinetic Data Evaluation Group [33]. The reaction scheme used for ethylene comprises 31 species and has 85 forward reaction steps. A full description can be found in Table 1, where the origin of the rate constants has also been indicated. Regarding propane flames the additional reaction steps suggested by Peters et al. [24] and Cernansky et al. [34] have been used, giving a total of 34 species and 111 forward reaction steps in this case. The additional reaction steps can be found in Table 2. All reverse reactions were computed by the use of JANAF [41] thermochemical data.

For a few of the reactions the earlier [29–32] rate constants formulated by Warnatz et al. have been used in the absence of a recommendation by the CEC group [33]. The steps concerned are mainly for recombination and decomposition reactions. However, in some cases older values were preferred on the basis of improved agreement with measurements in CH_4 and C_3H_8 counterflow diffusion flames. For example, the rate constant for the reaction describing the OH attack on C_2H_4 (reaction 47) the value recommended by Warnatz [31] was found to improve agreement significantly in CH_4 and C_3H_8 flames.

Data suitable for comparison with the gas-phase chemistry model include the CH_4 counterflow diffusion flames measured by Tsuji and Yamaoka [42] and Puri et al. [43]. Computations give excellent agreement with the measured major species. The agreement for the C_2 species is qualitatively correct and in particular predictions of C_2H_2 are very satisfactory. For propane–air flames the counterflow diffusion flame measured by Tsuji and Yamaoka [44] at a strain rate of 150/s was computed. All the above predictions were based on the assumption of adiabatic flames, an acceptable approximation as only small amounts of soot are present in these flames. The agreement with respect to pyrolysis products is excellent, as can be seen from Fig. 1. Furthermore, acetylene levels are again very well predicted. As a further check premixed C_2H_2 and C_2H_4 flames were computed, giving good agreement for burning velocities. However, it must be noted that uncertainties do remain relating to the accuracy of the current reaction mechanism. At present these particularly concern the quantitative prediction of a number of minor species, particularly for the propane flames. However, the predictions clearly display the correct qualitative trends and with respect to a number of features the quantitative predictions are also very satisfactory. Furthermore, for the current study it is probably sufficient that qualitative trends are well predicted by the gas-phase reaction mechanism to establish the validity of the soot model.

MODEL EQUATIONS

The calculation of the properties of counterflow flames involves the solution of the coupled mass conservation, momentum, energy, and species transport equations. For the counterflow geometry the governing equations and solution tech-

TABLE 1

Reaction Mechanism for C_1/C_2 Hydrocarbon Combustion. Rate Coefficient in the Form $k_f = AT^n \exp(-E/RT)^a$

	Reaction			A (m^3/kmol/s)	n	E (J/mol)	Ref.
1.	$H + O_2$	→	$OH + O$	0.200E + 12	0.0	0.703E + 05	33
2.	$O + H_2$	→	$OH + H$	0.512E + 02	2.67	0.263E + 05	33
3.	$OH + H_2$	→	$H_2O + H$	0.100E + 06	1.6	0.138E + 05	33
4.	$OH + OH$	→	$H_2O + O$	0.150E + 07	1.14	0.416E + 03	33
5.	$2H + M$	→	$H_2 + M$	0.980E + 11	−0.6	0.0	33
6.	$H + OH + M$	→	$H_2O + M$	0.220E + 17	−2.0	0.0	33
7.	$H + O_2 + M$	→	$HO_2 + M$	0.230E + 13	−0.8	0.0	33
8.	$H + HO_2$	→	$2OH$	0.168E + 12	0.0	0.366E + 04	33
9.	$H + HO_2$	→	$H_2 + O_2$	0.430E + 11	0.0	0.590E + 04	33
10.	$O + HO_2$	→	$OH + O_2$	0.320E + 11	0.0	0.0	33
11.	$OH + HO_2$	→	$H_2O + O_2$	0.290E + 11	0.0	0.208E + 04	33
12.	$CO + OH$	→	$CO_2 + H$	0.440E + 04	1.5	−0.308E + 04	33
13.	$CH_4 + H$	→	$CH_3 + H_2$	0.132E + 02	3.0	0.336E + 05	33
14.	$CH_4 + O$	→	$CH_3 + OH$	0.692E + 06	1.56	0.355E + 05	33
15.	$CH_4 + OH$	→	$CH_3 + H_2O$	0.156E + 05	1.83	0.116E + 05	33
16.	$CH_3 + H$	→	CH_4	0.190E + 34	−7.0	0.379E + 05	31
17.	$CH_3 + O$	→	$CH_2O + H$	0.843E + 11	0.0	0.0	33
18.	$CH_3 + OH$	→	$CH_2O + H_2$	0.800E + 10	0.0	0.0	43
19.	$CH_3 + CH_3$	→	C_2H_6	0.170E + 51	−12.0	0.812E + 05	31
20.	$CH_3 + CH_3$	→	$C_2H_5 + H$	0.800E + 12	0.0	0.111E + 06	31
21.	$CH_3 + CH_2$	→	$C_2H_4 + H$	0.400E + 11	0.0	0.0	33
22.	$CH_2 + H$	→	$CH + H_2$	0.600E + 10	0.0	−0.750E + 04	33
23.	$CH_2 + O$	→	$CO + 2H$	0.120E + 12	0.0	0.0	33
24.	$CH_2 + O_2$	→	$CO_2 + 2H$	0.313E + 11	0.0	0.0	33
25.	$CH_2 + C_2H_2$	→	$C_3H_3 + H$	0.180E + 10	0.0	0.0	31
26.	$CH_2 + C_2HO$	→	$C_2H_3 + CO$	0.200E + 11	0.0	0.0	30
27.	$CH_2O + H$	→	$CHO + H_2$	0.230E + 08	1.05	0.137E + 05	33
28.	$CH_2O + O$	→	$CHO + OH$	0.415E + 09	0.57	0.116E + 05	33
29.	$CH_2O + OH$	→	$CHO + H_2O$	0.343E + 07	1.18	−0.187E + 04	33
30.	$CH + O$	→	$CO + H$	0.400E + 11	0.0	0.0	33
31.	$CH + O_2$	→	$CO + OH$	0.330E + 11	0.0	0.0	33
32.	$CH + C_2H_2$	→	C_3H_3	0.190E + 11	0.0	0.0	31
33.	$CHO + H$	→	$CO + H_2$	0.900E + 11	0.0	0.0	33
34.	$CHO + O$	→	$CO + OH$	0.300E + 11	0.0	0.0	33
35.	$CHO + O$	→	$CO_2 + H$	0.300E + 11	0.0	0.0	33
36.	$CHO + OH$	→	$CO + H_2O$	0.102E + 12	0.0	0.0	33
37.	$CHO + O_2$	→	$CO + HO_2$	0.300E + 10	0.0	0.0	33
38.	$CHO + M$	→	$CO + H + M$	0.250E + 12	0.0	0.703E + 05	33
39.	$C_2H_6 + H$	→	$C_2H_5 + H_2$	0.144E + 07	1.5	0.310E + 05	33
40.	$C_2H_6 + O$	→	$C_2H_5 + OH$	0.100E + 07	1.5	0.243E + 05	33
41.	$C_2H_6 + OH$	→	$C_2H_5 + H_2O$	0.723E + 04	2.0	0.362E + 04	33
42.	$C_2H_5 + O$	→	$C_2H_4O + H$	0.843E + 11	0.0	0.0	33
43.	$C_2H_5 + O_2$	→	$C_2H_4 + HO_2$	0.102E + 08	0.0	−0.915E + 04	33
44.	C_2H_5	→	$C_2H_4 + H$	0.100E + 44	−9.1	0.244E + 06	24
45.	$C_2H_4 + H$	→	$C_2H_3 + H_2$	0.542E + 12	0.0	0.628E + 05	33
46.	$C_2H_4 + O$	→	$CHO + CH_3$	0.350E + 04	2.08	0.0	33
47.	$C_2H_4 + OH$	→	$C_2H_3 + H_2O$	0.700E + 11	0.0	0.126E + 05	31
48.	$C_2H_4 + OH$	→	$CH_3 + CH_2O$	0.199E + 10	0.0	0.402E + 04	34
49.	$C_2H_4O + H$	→	$C_2H_3O + H_2$	0.409E + 07	1.16	0.100E + 05	33
50.	$C_2H_4O + O$	→	$C_2H_3 + OH$	0.580E + 10	0.0	0.760E + 04	33
51.	$C_2H_4O + OH$	→	$C_2H_3O + H_2O$	0.235E + 08	0.73	−0.465E + 04	33
52.	$C_2H_3 + H$	→	$C_2H_2 + H_2$	0.120E + 11	0.0	0.0	33
53.	$C_2H_3 + O$	→	$C_2H_2O + H$	0.300E + 11	0.0	0.0	32
54.	$C_2H_3 + O_2$	→	$CH_2O + CHO$	0.540E + 10	0.0	0.0	33

TABLE 1 Continued

	Reaction			A (m^3/kmol/s)	n	E (J/mol)	Ref.
55.	C_2H_3	→	$C_2H_2 + H$	0.530E + 29	−5.5	0.194E + 06	24
56.	$C_2H_3O + M$	→	$CH_3 + CO + M$	0.100E + 13	0.0	0.394E + 05	29
57.	$C_2H_2 + H$	→	$C_2H + H_2$	0.600E + 11	0.0	0.116E + 06	33
58.	$C_2H_2 + O$	→	$CH_2 + CO$	0.217E + 02	2.8	0.208E + 04	33
59.	$C_2H_2 + O$	→	$C_2HO + H$	0.217E + 02	2.8	0.208E + 04	33
60.	$C_2H_2 + OH$	→	$C_2H_2O + H$	0.600E + 11	0.0	0.540E + 05	33
61.	$C_2H_2 + OH$	→	$C_2H + H_2O$	0.600E + 11	0.0	0.540E + 05	33
62.	$C_2H_2O + H$	→	$CH_3 + CO$	0.180E + 11	0.0	0.140E + 05	33
63.	$C_2H_2O + O$	→	CHC + CHO	0.230E + 10	0.0	0.570E + 04	33
64.	$C_2H_2O + OH$	→	$CH_2O + CHO$	0.100E + 11	0.0	0.0	33
65.	$C_2H_2O + M$	→	$CH_2 + CO + M$	0.100E + 14	0.0	0.248E + 06	32
66.	$C_2H_2O + O$	→	CO + CH	0.100E + 11	0.0	0.0	33
67.	$C_2H + O_2$	→	CO + CHO	0.500E + 11	0.0	0.630E + 04	31
68.	$C_2H + C_2H_2$	→	$C_4H_2 + H$	0.350E + 11	0.0	0.0	31
69.	$C_2HO + H$	→	$CH_2 + CO$	0.300E + 11	0.0	0.0	31
70.	$C_2HO + O$	→	2CO + H	0.100E + 12	0.0	0.0	33
71.	$C_3H_4 + H$	→	$C_3H_3 + H_2$	0.500E + 10	0.0	0.628E + 04	48
72.	$C_3H_4 + O$	→	$CH_2O + C_2H_2$	0.100E + 10	0.0	0.0	24
73.	$C_3H_4 + O$	→	$C_2H_3 + CHO$	0.100E + 10	0.0	0.0	24
74.	$C_3H_4 + OH$	→	$C_2H_4 + CHO$	0.100E + 10	0.0	0.0	24
75.	$C_3H_4 + OH$	→	$C_2H_3 + CH_2O$	0.100E + 10	0.0	0.0	24
76.	C_3H_4	→	$C_3H_3 + H$	0.500E + 15	0.0	0.370E + 06	24
77.	$C_3H_3 + O$	→	$C_3H_2 + OH$	0.320E + 10	0.0	0.0	30
78.	$C_3H_3 + O$	→	$CO + C_2H_3$	0.380E + 11	0.0	0.0	31
79.	$C_3H_3 + O_2$	→	$C_2HO + CH_2O$	0.600E + 10	0.0	0.0	32
80.	$C_3H_2 + H$	→	C_3H_3	0.600E + 10	0.0	0.0	30
81.	$C_3H_2 + O$	→	$C_2H + CHO$	0.680E + 11	0.0	0.0	30
82.	$C_3H_2 + OH$	→	$C_2H_2 + CHO$	0.680E + 11	0.0	0.0	30
83.	$C_4H_2 + O$	→	$C_3H_2 + CO$	0.270E + 11	0.0	0.720E + 04	30
84.	$C_4H_2 + OH$	→	$C_3H_2 + CHO$	0.300E + 11	0.0	0.0	30
85.	$C_4H_2 + C_2H$	→	$C_6H_2 + H$	0.350E + 11	0.0	0.0	31

[a][M] = 1.0[FUEL] + 6.0[H_2O] + 1.0[H_2] + 1.5[CO_2] + 0.4[N_2] + 0.4[O_2].

niques have been outlined elsewhere [25, 26] and are not repeated here.

$$\frac{\partial V}{\partial \eta} + \Phi' = 0,$$

$$\frac{1}{a}\frac{\partial \Phi'}{\partial t} + V\frac{\partial \Phi'}{\partial \eta} = \frac{\partial}{\partial \eta}\left(\mu'\frac{\partial \Phi'}{\partial \eta}\right) + \left(\frac{1}{\rho'} - \Phi'\right),$$

$$\frac{1}{a}\frac{\partial Y_k}{\partial t} + V\frac{\partial Y_k}{\partial \eta} = -\frac{\partial J_k}{\partial \eta} + \frac{R_k M_k}{\rho a},$$

$$\frac{1}{a}\frac{\partial N}{\partial t} + V\frac{\partial N}{\partial \eta} = -\frac{\partial J_N}{\partial \eta} + \frac{R_N}{\rho a},$$

$$\frac{1}{a}\frac{\partial h}{\partial t} + V\frac{\partial h}{\partial \eta} = \frac{\partial}{\partial \eta}\left(\frac{\mu'}{\sigma_{\mathrm{Pr}}}\frac{\partial h}{\partial \eta}\right) + \frac{\partial}{\partial \eta}\left(\sum_{k=1}^{n_{\mathrm{sp}}} h_k\left(-J_k - \frac{\mu'}{\sigma_{\mathrm{Pr}}}\frac{\partial Y_k}{\partial \eta}\right)\right),$$

and where

$$R_k = \sum_{j=1}^{n_{\mathrm{reac}}} \Xi_{jk}\left(k_j^f \prod_{l=1}^{n_{\mathrm{sp}}} \phi_l \xi_{jk} - k_j^r \prod_{l=1}^{n_{\mathrm{sp}}} \phi_l \xi_{jk}\right),$$

$$\Phi' = \frac{u}{u_e'}\mu' = \frac{\rho\mu}{\rho_e \mu_e'}\rho' = \frac{\rho}{\rho_e'}V = \frac{\rho v}{\sqrt{\rho_e \mu_e a}},$$

$$\eta = \sqrt{\frac{a}{\rho_e \mu_e}}\int_0^y \rho\, dy,$$

and where u and v are the components of velocity in the x and y direction, respectively, ρ is the fluid density, μ is the fluid viscosity, y_k is the mass fraction and M_k is the molar mass of specie k, h is the mixture enthalpy, N is the particle number density, a is the strain rate, and t is time. The subscript e denotes values prevailing in the potential flow at the edge of the boundary

TABLE 2

Reaction Mechanism for C_3 Hydrocarbon Combustion. Rate Coefficient in the Form $k_f = AT^n \exp(-E/RT)$

	Reaction			A (m^3/kmol/s)	n	E (J/mol)	Ref.
86.	C_3H_8	→	$C_2H_5 + CH_3$	0.300E + 23	−1.8	0.371E + 06	51
87.	$C_3H_8 + H$	→	$n\text{-}C_3H_7 + H_2$	0.130E + 12	0.0	0.406E + 05	31
88.	$C_3H_8 + H$	→	$i\text{-}C_3H_7 + H_2$	0.100E + 12	0.0	0.349E + 05	31
89.	$C_3H_8 + O$	→	$n\text{-}C_3H_7 + OH$	0.300E + 11	0.0	0.241E + 05	31
90.	$C_3H_8 + O$	→	$i\text{-}C_3H_7 + OH$	0.260E + 11	0.0	0.187E + 05	31
91.	$C_3H_8 + OH$	→	$n\text{-}C_3H_7 + H_2O$	0.370E + 10	0.0	0.690E + 04	31
92.	$C_3H_8 + OH$	→	$i\text{-}C_3H_7 + H_2O$	0.280E + 10	0.0	0.360E + 04	31
93.	$n\text{-}C_3H_7 + H$	→	C_3H_8	0.200E + 11	0.0	0.0	31
94.	$i\text{-}C_3H_7 + H$	→	C_3H_8	0.200E + 11	0.0	0.0	31
95.	$n\text{-}C_3H_7 + O_2$	→	$C_3H_6 + HO_2$	0.100E + 10	0.0	0.209E + 05	31
96.	$i\text{-}C_3H_7 + O_2$	→	$C_3H_6 + HO_2$	0.100E + 10	0.0	0.125E + 05	31
97.	$n\text{-}C_3H_7$	→	$C_2H_4 + CH_3$	0.888E + 12	0.0	0.127E + 06	51
98.	$n\text{-}C_3H_7$	→	$C_3H_6 + H$	0.135E + 12	0.0	0.127E + 06	51
99.	$i\text{-}C_3H_7$	→	$C_2H_4 + CH_3$	0.177E + 12	0.0	0.149E + 06	51
100.	$i\text{-}C_3H_7$	→	$C_3H_6 + H$	0.166E + 13	0.0	0.149E + 06	51
101.	$C_3H_6 + H$	→	$C_3H_5 + H_2$	0.112E + 11	0.0	0.0	49
102.	$C_3H_6 + O$	→	$2CH_3 + CO$	0.500E + 10	0.0	0.190E + 04	31
103.	$C_3H_6 + OH$	→	$C_2H_4O + CH_3$	0.100E + 11	0.0	0.0	31
104.	$C_3H_6 + OH$	→	$C_3H_5 + H_2O$	0.200E + 11	0.0	0.128E + 05	34
105.	$C_3H_6 + O_2$	→	$C_3H_5 + HO_2$	0.100E + 12	0.0	0.161E + 06	34
106.	C_3H_6	→	$C_2H_3 + CH_3$	0.820E + 13	0.0	0.335E + 06	50
107.	C_3H_6	→	$C_3H_5 + H$	0.350E + 13	0.0	0.314E + 06	50
108.	$C_3H_5 + H$	→	$C_3H_4 + H_2$	0.100E + 11	0.0	0.0	24
109.	$C_3H_5 + O_2$	→	$C_3H_4 + HO_2$	0.600E + 09	0.0	0.419E + 05	24
110.	$C_3H_5 + CH_3$	→	$C_3H_4 + CH_4$	0.500E + 09	0.0	0.0	34
111.	C_3H_5	→	$C_3H_4 + H$	0.398E + 14	0.0	0.293E + 06	24

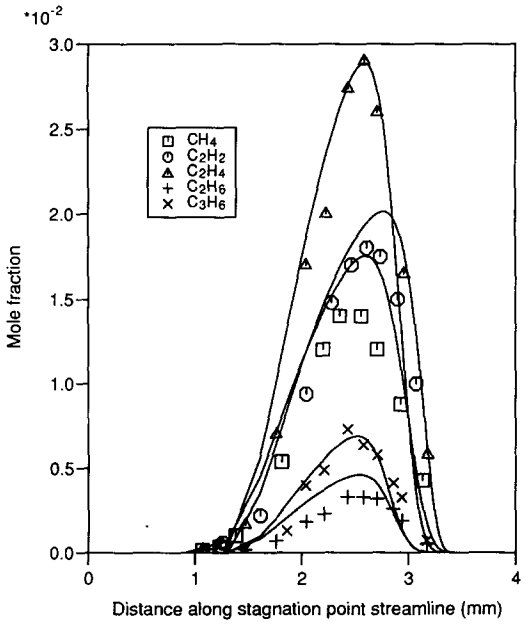

Fig. 1. Prediction of intermediate hydrocarbons in a counterflow C_3H_8-air diffusion flame at a strain rate of 150/s. Measurements from Tsuji and Yamaoka [44].

layer. The expression for the flux terms has recently been discussed elsewhere [25, 26] and may, for the gaseous species, be written as

$$J_k = -\frac{\mu'}{\sigma_{Sc}}\left(\frac{\partial Y_k}{\partial \eta} - y_k \frac{1}{n}\frac{\partial n}{\partial \eta}\right) - \frac{v_c}{v} V Y_k.$$

For soot particles only thermophoretical transport [16] is considered, and the corresponding additional velocity term may be written as

$$V_t = -0.55 \frac{\rho\mu}{\rho_e \mu_e} \frac{1}{T}\frac{\partial T}{\partial \eta}.$$

Furthermore, the computed flames are typically not adiabatic and exhibit an incorrect temperature profile in the absence of heat loss. Kennedy et al. [7] implemented a heat-loss term based on the assumption of an optically thin medium and considered only radiation from the formed soot but not from gaseous species. While this approach may have some advantages and can be readily implemented a simpler approach was

adopted in the present work. This is based on matching the experimental temperature profile of Fairweather et al. [3] and Moss et al. [9] by the introduction of a heat loss factor. Consequently for each flame the temperature was adjusted from the adiabatic value (T_{ad}) by assuming the following relationship,

$$T = T_{ad}\left(1 - \beta\left(\frac{T_{ad}}{T_{max}}\right)^4\right).$$

The subscript "ad" denotes the adiabatic condition and "max" the maximum *adiabatic* temperature. Different heat loss fractions (β) in the range $0.09 < \beta < 0.15$ were tested but it was found that for all ethylene flames a value of 0.12 and for all propane flames a value of 0.09 gave acceptable agreement with measured temperature profiles. An example can be found for selected ethylene flames in Fig. 2. The discrepancy in the vicinity of the stagnation point is an indication of some degree of preheating of the fuel, and the possible consequences are discussed in the results section below.

The above equation system has been solved using an implicit difference formulation involving two-point backward time differencing and central differences for the spatial derivatives. Further details can be found in Jones and Lindstedt [25, 26].

Mesh distributions were set to concentrate nodes in the regions of maximum change in species profiles, with particular care taken to resolve the soot formation regions of the flames. Typically a minimum of 87 distributed nodes was used to start a computation with a minimum of 109 distributed nodes used in the final solution. For the cases tested further grid refinement was found not to effect the final results appreciably.

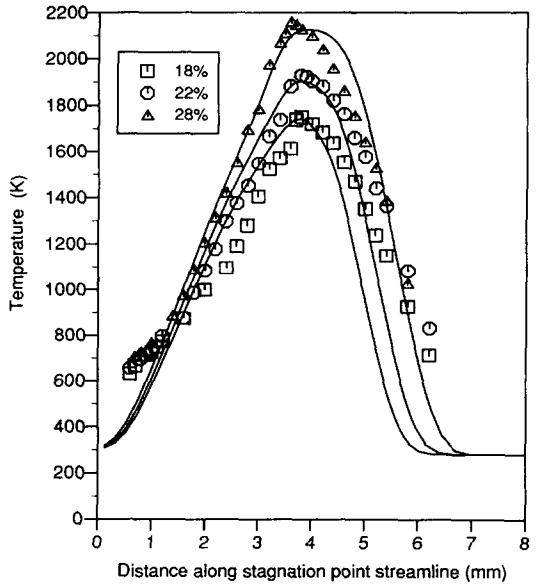

Fig. 2. Temperature profiles for counterflow C_2H_4-O_2-N_2 flames with varying O_2 concentrations. Measurements by Vandsburger et al. [21].

RESULTS AND DISCUSSION

The first set of computations were of a C_2H_4 flame burning with an oxidant stream of 22 mol.% oxygen and 78 mol.% nitrogen. The velocity gradient $2V/R$ (rate of strain) of 63/s (estimated by Vandsburger et al. [21]) was applied with a fuel injection velocity of 0.10 m/s. These computations served to determine the appropriate preexponential factors in the nucleation and soot surface growth steps as outlined above.

Vandsburger et al. [21] also measured flames with varying mole fractions of O_2 in the air stream with values ranging from 0.18 to 0.28. Date from these flames were used to establish the generality of the present model, and comparisons were made without further adjustments to any of the constants in either the gas phase or the soot models. These flames provide a very stern test, as both peak temperatures and in particular acetylene levels vary greatly with oxygen concentrations in the oxidant stream. The computed acetylene and polyacetylene profiles for three of the five different flames are plotted against mixture-fraction in Fig. 3. As can be seen, the peak level of C_2H_2 varies by around a factor of 2. It can be shown as part of a systematic reduction of the C_2 mechanism [28] that the polyacetylenes C_4H_2 and C_6H_2 are in partial equilibrium with C_2H_2. However, the absolute levels (as mass-fractions) are significantly lower than that of soot, as suggested by Harris and Weiner [13, 14].

The range of peak temperature recorded in the flames, from 1750 to 2150 K, is also large. These variations are similar to, or in excess of those encountered when an initially unstrained counterflow alkane-air diffusion flame is strained to extinction.

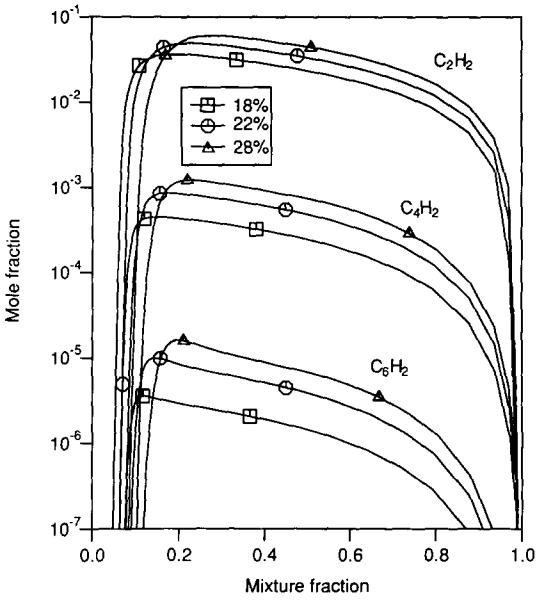

Fig. 3. Predicted acetylene and polyacetylene mole-fractions in counterflow C_2H_4-O_2-N_2 flames with varying O_2 concentrations as functions of mixture fraction.

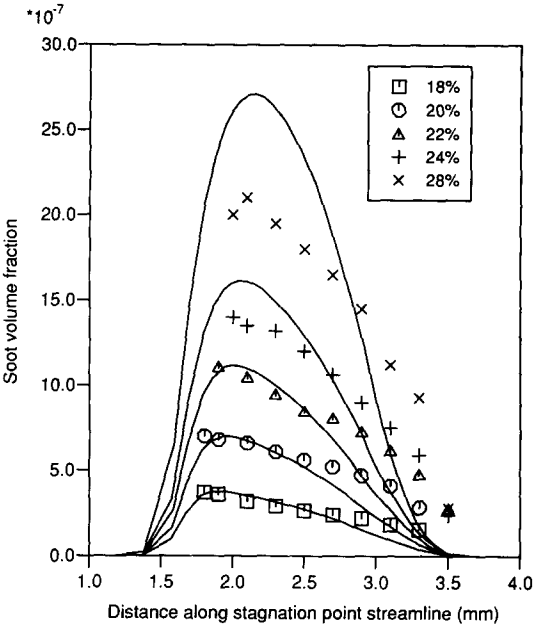

Fig. 4. Predicted soot volume fractions for counterflow C_2H_4-O_2-N_2 flames with varying O_2 concentrations. Measurements by Vandsburger et al. [21].

The predicted soot volume fractions in the different flames can be seen from Fig. 4. The agreement between the model and the experimental data must be regarded as very good, and the maximum errors in soot levels are generally around 20%, with the largest errors occurring for the most oxygen-enriched flame. Thus while the predicted peak soot volume fraction for the flame with the lowest oxygen concentration (0.18) was $3.8*10^{-7}$, compared with the measured value of $3.7*10^{-7}$, the flame with the highest oxygen concentration (0.28) gave a predicted peak level of $2.7*10^{-6}$, compared with the measured level of $2.1*10^{-6}$. For the other flames the agreement between predictions and measurements is more satisfactory. The discrepancies are sufficiently small to be attributable to uncertainties in the gas-phase chemistry model and the simplified treatment of nonadiabaticity via a constant heat loss factor for all flames. For the latter it would be more accurate to include radiation from the soot layer in the flame. However, further improvements are also likely to be required in the treatment of the surface growth step.

It is also interesting to view the correlation of soot formation rates agains t temperature and mixture fraction for a typical flame. In Fig. 5 the to tal soot formation rate for the 22% O_2 flame is shown as a function of total mixture fraction and temperature. Several interesting features are clear. Firstly, the location of the maximum growth rate is shifted well to the rich side of the flame and occurs at a mixture fraction of around 0.17. It is also clear that the soot formation rate has dropped by an order of magnitude at around 1300 K and two orders of magnitude at around 1000 K. This behavior is plausible and in agreement with experimental studies, for example, Kent and Honnery [18]. For cooler flames with less oxygen enrichment, the point of maximum soot mass growth moves progressively towards leaner mixtures as the temperature drops on the fuel side of the flame, while the opposite is true for the hotter, more oxygen enriched, flames. A more complete list of parameters can be found in Table 3, where peak temperatures and C_2H_2 concentrations at the location of maximum rate of soot growth are shown along with the peak specific surface growth rate obtained in the flames. It can in addition be seen from Table 3 that there is a significant increase in acetylene concentrations, from 0.0347 to 0.0557, for these flames. As a consequence the peak soot formation rate varies by almost an order of magnitude. Thus the range of maximum soot formation rates deduced from

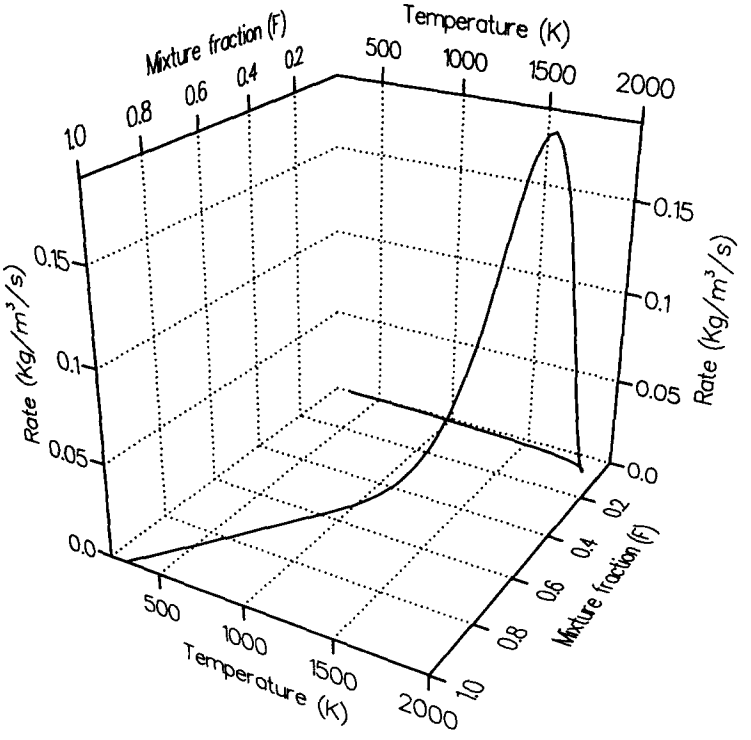

Fig. 5. Sum of predicted nucleation and surface growth rates for a C_2H_4-O_2-N_2 flame plotted as a function of mixture fraction and temperature.

the model were from $5.9*10^{-2}$ to $5.3*10^{-1}$ kg/m^3/s for oxygen indices from 0.18 to 0.28. This compares well with the range deduced from experiments [21], which was found to be from $3.8*10^{-2}$ to $8.8*10^{-1}$ kg/m^3/s. It can also be noted that Vandsburger et al. [21] give a value of $5.2*10^{-1}$ kg/m^3/s a short distance away from the flame front for the hottest flame and part of the discrepancies may thus be due to experimental uncertainties.

It is clear that the maximum formation rates obtained in the counterflow geometry are significantly lower than those observed by Kent and Honnery [18] in co-flowing axisymmetric flames where a peak value of around 1.25 kg/m^3/s was estimated. The predicted maximum destruction rates are also significantly lower in the counterflow geometry due to the different flame structure. In this context it should also be noted that the maximum soot volume fractions of $1.8*10^{-5}$ in the co-flowing flames measured by Kent and Honnery [18] are also accordingly significantly higher. This soot volume fraction is also appreciably higher than the value of $6.0*10^{-6}$ measured by Kent and Wagner [16] in a Wolfhard-Parker burner. These values in co-flowing flames can be compared with the presently computed counterflow configuration corresponding to an oxygen

TABLE 3

Mole-fractions of C_2H_2 ($x_{C_2H_2}$), Temperature [$T(K)$], and Mixture Fraction (f) at the Location of the Peak Soot Formation Rate ($\langle R_p \rangle$) for C_2H_4 and C_3H_8 flames. Also Shown is the Maximum Surface Specific Soot Formation Rate $\langle R_s \rangle$ (m/s)

Flame	$\langle R_p \rangle$	$\langle R_s \rangle$	$X_{C_2H_2}$	f	T
C_2H_4/0.18 O_2	$5.92*10^{-2}$	$1.67*10^{-6}$	0.0347	0.144	1577
C_2H_4/0.20 O_2	$1.14*10^{-1}$	$1.63*10^{-6}$	0.0415	0.162	1623
C_2H_4/0.22 O_2	$1.89*10^{-1}$	$1.64*10^{-6}$	0.0447	0.166	1697
C_2H_4/0.24 O_2	$2.85*10^{-1}$	$1.74*10^{-6}$	0.0500	0.187	1722
C_2H_4/0.28 O_2	$5.30*10^{-1}$	$1.71*10^{-6}$	0.0557	0.220	1785
C_3H_8/0.24 O_2	$1.01*10^{-1}$	$2.42*10^{-6}$	0.0194	0.103	1675
C_3H_8/0.28 O_2	$2.13*10^{-1}$	$2.38*10^{-6}$	0.0248	0.128	1710

mole-fraction of 0.2089 in the oxidant stream, which yields a predicted peak soot volume fraction of around $1.0*10^{-6}$, a value entirely consistent with those observed in co-flowing flames.

Arguably a more appropriate measure of the behavior of the model is the specific growth rate that has been normalized by the surface area available locally in the flame. This property is plotted in Fig. 6, where the measurements by Vandsburger et al. [21] are also shown. The agreement between measurements and predictions is generally acceptable, particularly for the hotter parts of the flame. In the latter region the predictions appear to be within experimental uncertainties. Moving away from the flame front a decrease of specific surface growth rate of about an order of magnitude is observed, which is roughly in accordance with measurements. Furthermore, the experimentally observed trend that the specific surface growth rate increases more rapidly close to the flame front with mole-fraction of O_2 in the oxidant stream is also obtained. However, an interesting feature, clearly visible from Table 3, is that the peak surface specific growth rate remains essentially constant for all the ethylene flames.

The predictions of soot number densities (Fig. 7) are arguably less satisfactory, though the trends appear well predicted by the model. Furthermore, there are considerable uncertainties in the measured particle number densities, as such measurements are extremely time consuming and difficult to perform. Vandsburger et al. [21] noted that the assumption that the particles constitute a monodisperse spray does not apply to a coagulating aerosol and that the assumption of a log-normal size distribution would decrease the mean diameter by up to 50% and increase the particle number density around eightfold. With these reservations the predicted particle number densities are well within the range of 10^{16}-10^{17} particles/m^3 observed experimentally.

However, it is evident, perhaps as expected, that the simplified coagulation expression used does not represent the process accurately over the entire range of conditions. The measurements indicate that freshly formed particles have a significantly higher rate of coagulation than older particles. Furthermore, it appears clear from the measurements [21] that older particles in the cold part of the flame essentially do not agglomerate. Wagner [12] has suggested that the type of rate expression used in the current model accurately

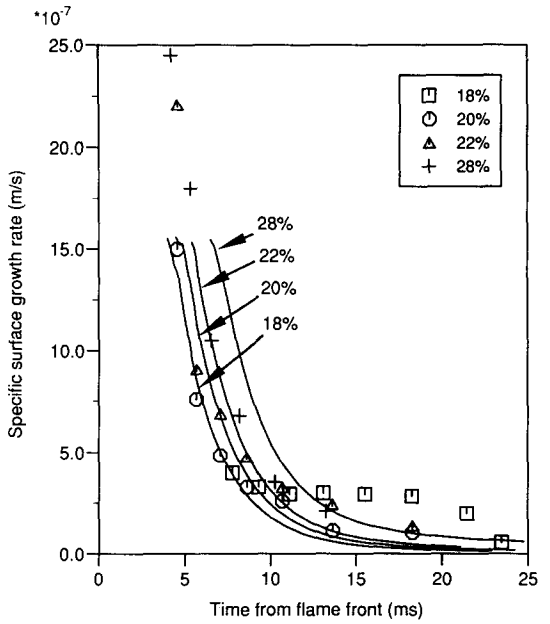

Fig. 6. Predicted soot formation rates for counterflow C_2H_4-O_2-N_2 flames with varying O_2 concentrations normalized by surface area. Measurements by Vandsburger et al. [21].

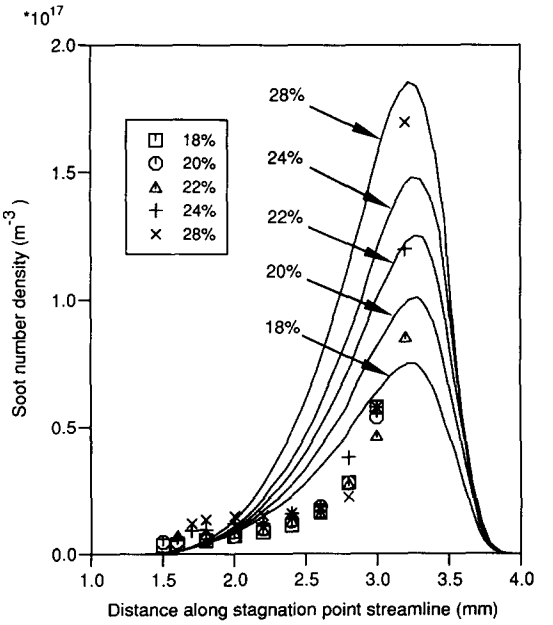

Fig. 7. Predicted soot number densities for counterflow C_2H_4-O_2-N_2 flames with varying O_2 concentrations. Measurements by Vandsburger et al. [21].

predicts the behavior of sprays up to particle sizes of around 300 nm. The current study appears to suggest that the range of applicability in the counterflow flame geometry is more limited. However, the model does yield good results both qualitatively and quantitatively for particle sizes up to around 70 nm for the five flames predicted, as can be seen from Fig. 8. At later stages the simplified coagulation rate expression appears to exaggerate the rate of growth, though it should be noted that this occurs close to the stagnation point and at low flame temperatures below 900 K. Nevertheless, it appears clear that an improved description of the change in particle number densities throughout the flame would be beneficial.

The predicted temperature profiles for the two propane flames with oxygen mole-fractions in the oxidant stream of 0.24 and 0.28, respectively, are similar to those shown for the ethylene flames. Again the agreement is satisfactory other than in the vicinity of the burner, where the predicted temperatures are considerably lower than those measured. The reason for this discrepancy is not clear, though it should be noted that for essentially nonsooting flames it does not occur. For example, the temperature profiles measured by Tsuji and Yamaoka [42] for methane–air flames are well reproduced in this region. The discrepancy is not too significant in the model evaluation for a single fuel as the temperature profiles for all flames merge in this region. However, preheating of different fuels may have appreciably different effects on their pyrolysis behavior close to a burner, as clearly noted in co-flowing flames [52]. This gives rise to an additional source of uncertainty in the determination of the rate constant for surface growth.

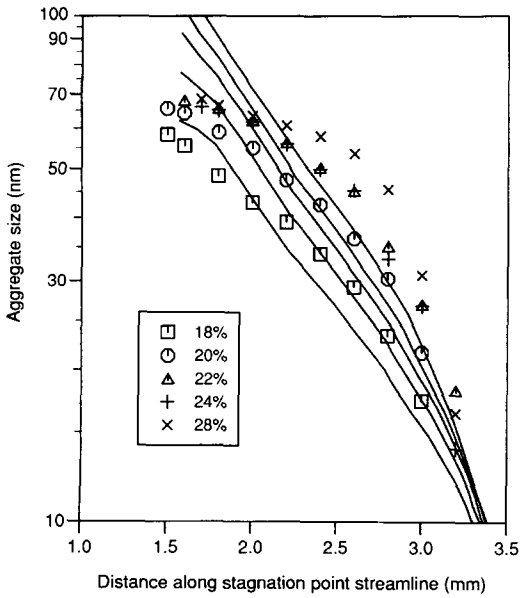

Fig. 8. Predicted aggregate sizes for counterflow C_2H_4-O_2-N_2 flames with varying O_2 concentrations. Measurements by Vandsburger et al. [21].

For optimal predictions of soot volume fractions in both propane flames it was found necessary to increase the preexponential factor in the surface growth rate expression from $0.60*10^4$ to $0.12*10^5$. This is naturally not desirable. One possible contributing cause, as discussed above, is the difference in pryolysis behavior caused by preheating of the fuel. However, this is not expected to be a major cause in the counterflow geometry and it cannot be ruled out that the assumption of incipient particle formation being dependent on acetylene concentrations rather than the formation of (poly-)aromatic hydrocarbons in the flame is too simplified. Still the adjustment of the preexponential factor is arguably within the uncertainties of the gas-phase reaction mechanism, although it is more likely that the former reasons are the major cause of the necessary adjustment. The soot volume fractions can be found in Fig. 9, where results of comparable quality to those observed for the ethylene flames are shown; the agreement between measurements and predictions is again very good and any discrepancies are probably within measurement uncertainties.

The predicted peak soot formation rates in the two flames are $1.0*10^{-1}$ and $2.1*10^{-1}$ kg/m^3/s for the case 0.24 and 0.28 mole-fraction of O_2 in the oxidant stream respectively. The corresponding values obtained from experimental observations [21] were $2.4*10^{-1}$ and $2.8*10^{-1}$ kg/m^3/s, respectively. Although there are differences the agreement is satisfactory. The values obtained for the propane flames are roughly one third of those recorded in ethylene flames with the same oxidant streams, as can be seen from Table 3. It is also shown in Table 3 that the location of maximum soot mass growth occurs at lower values of mixture fraction for the propane flames than for the ethylene flames. This is consistent with the lower peak temperature observed for the propane flames. The peak acetylene concentrations in the two

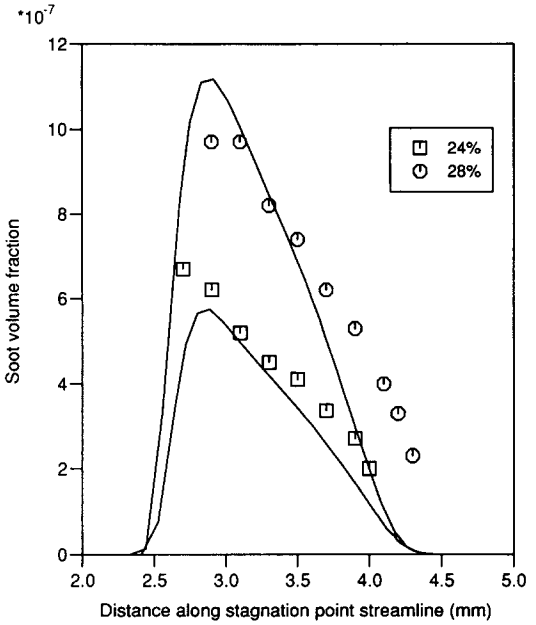

Fig. 9. Predicted soot volume fractions for counterflow C_3H_8-O_2-N_2 flames with varying O_2 concentrations. Measurements by Vandsburger et al. [21].

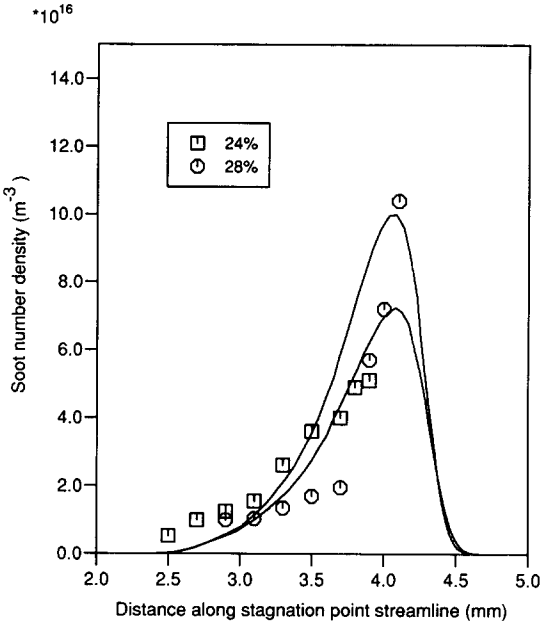

Fig. 10. Predicted soot number densities for counterflow C_3H_8-O_2-N_2 flames with varying O_2 concentrations. Measurements by Vandsburger et al. [21].

flames also varies from 2.36% to 2.91% and the variation in the peak temperature is from 1927 to 2065 K.

Regarding predictions of soot number densities (Fig. 10), these are predicted satisfactorily without need for any model adjustment. The growth in soot particle size (Fig. 11) shows the same behavior as in the ethylene flames and it can be seen that the agreement obtained for the cooler flame is very good for both particle number density and growth in particle size. However, the measurements indicate that a constant particle size of around 70 nm is approached. This is, as discussed above, a significantly lower value than that predicted by the current standard model used in this and other investigations [12, 16, 18].

The extent of the region of particle formation could also influence the particle size in the early part of the flame. The width of region of maximum particle formation in the current flames is of the order 1 mm or less. This value is in good agreement with that observed experimentally [21]. It would therefore appear that the agglomeration of particles requires an improved description in this respect, and studies of the behavior of non-reacting aerosols of Harris and Kennedy [53] provide useful information.

CONCLUSIONS

A simplified reaction model for soot formation has been proposed and tested for a wide range of counterflow C_2H_4-O_2-N_2 and C_3H_8-O_2-N_2

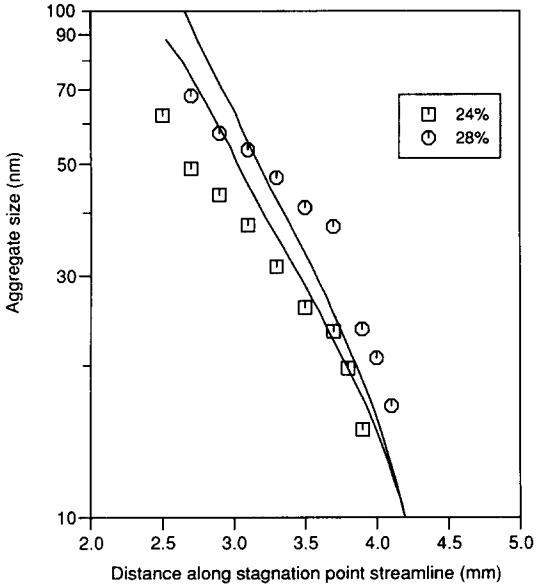

Fig. 11. Predicted aggregate sizes for counter-flow C_3H_8-O_2-N_2 flames with varying O_2 concentrations. Measurements by Vandsburger et al [21].

flames. The model is based on the use of a characteristic pyrolysis product, C_2H_2, to link the gas-phase chemistry to the soot formation steps. To evaluate the soot mechanism it was combined with detailed gas-phase chemistry with up to 111 forward reaction steps. However, the inherent simplicity of the approach also opens up considerable scope for the introduction of simplified description of gas-phase chemistry.

The soot model requires solution of conservation equations for the soot mass-fraction and number density. The model is closed by the assumption of a spherical particle shape.

The agreement obtained with the model is very encouraging. Errors in predictions of soot volume fractions using the model are of the same order as the uncertainties associated with experimental data, the detailed reaction mechanism used for the prediction of C_2H_2 concentration profiles, and the simplified treatment of nonadiabaticity. Furthermore, predictions of other properties such as particle number densities and aggregate sizes are also satisfactory.

However, further work is desirable in order to generalize the model. Such work should include a more realistic description of soot oxidation incorporating an oxidation step dependent on OH radical concentrations. Although this is not a particularly important feature in the counterflow geometry, due to the resulting flame structure, it is of greater importance in co-flowing flames. Improvements in the modeling of soot particle formation, possibly via aromatic species, as well as improvements in the current model for adsorption of growth species on active sites, are also likely to contribute to a more general model. Work is currently in progress in all of these areas.

The authors wish to gratefully acknowledge the financial support of British Gas plc and SERC under co-funded award GR/D/07749 and the Ministry of Defense at RAE Pyestock for parts of this work.

REFERENCES

1. Frenklach, M., Clary, D. W., Gardiner, W. C., and Stein, S. E., *Twentieth Symposium (International) on Combustion*, The Combustion Institute, 1984, pp. 887-901.
2. Frenklach, M. and Wang, H. Presented at the Twenty-Third Symposium (International) on Combustion, Orleans, July 1990.
3. Fairweather, M., Jones, W. P., and Lindstedt, R. P., submitted to Combust. and Flame (1991).
4. Jones, W. P., and Kollmann, W., *Turbulent Shear Flows 5*, Springer Verlag, Berlin, 1987.
5. Tesner, P. A., Snegiriova, T. D., and Knorre, V. G., *Combustion Flame* 17:253 (1971).
6. Gilyazefdinov, L. P., *Khim. Tverd. Topl.* 3:103 (1972).
7. Kennedy, I., Kollmann, W., and Chen, Y., Presented at the 28th Aerospace Science Meeting, January 1990, Paper AIAA 90-0456.
8. Magnussen, B. F., *Seventeenth Symposium (International) on Combustion*. The Combustion Institute, 1979, pp. 1383-1397.
9. Moss, J. B., Stewart, C. D., and Syed, K. J., *Twenty-Second Symposium (International) on Combustion*, The Combustion Institute, 1988, p. 413.
10. Syed, K. J., Stewart, C. D., and Moss, J. B., Presented at Twenty-Third Symposium (International) on Combustion, Orleans, July 1990.
11. Flower, W. L., and Bowman, C. T., *Twenty-First Symposium (International) on Combustion*, The Combustion Institute, 1986, pp. 1115-1124.
12. Wagner, H. Gg., Invited Lecture, *Eighteenth Symposium (International) on Combustion*, The Combustion Institute, 1980, pp. 3-19.
13. Harris, S. J., and Weiner, A. M., *Combust. Sci. Technol.* 31:155 (1983).
14. Harris, S. J., and Weiner, A. M., *Combust. Sci. Technol.* 32:267-275 (1983).
15. Smyth, K. C., Miller, J. H., Dorfman, R. C., Mallard, W. G., and Santoro, R. J., *Combust. Flame* 62:157-181 (1985).
16. Kent, J. H., and Wagner, H. Gg., *Combust. Flame* 47:53-65 (1982).
17. Miller, J. H., Mallard, W. G., and Smyth, K. C., *Twenty-First Symposium (International) on Combustion*, The Combustion Institute, 1986, pp. 1057-1065.
18. Kent, J. H., and Honnery, D. R., *Combust. Flame* 79:287-298 (1990).
19. Kent, J. H., and Bastin, S. J., *Combust. Flame* 56: 29-42 (1984).
20. Becker, H. F., and Yamazaki, S., *Sixteenth Symposium (International) on Combustion*, The Combustion Institute, 1977, pp. 681-690.
21. Vandsburger, U., Kennedy, I., and Glassman, I., *Combust. Sci. Technol.* 39:263-285 (1984).
22. Hura, H. S., and Glassman, I., *Combust. Sci. Technol.* 53:1-21 (1987).
23. Miller, J. A., Presented at the Twenty-Third Symposium (International) on Combustion, Orleans, July 1990.
24. Peters, N., Mauss, F., and Warnatz, J., Presented at the Twenty-Third Symposium (International) on Combustion, Orleans, July 1990.
25. Jones, W. P., and Lindstedt, R. P., *Combust. Flame* 73:233 (1988).
26. Jones, W. P., and Lindstedt, R. P., *Combust. Sci. Technol.* 61:31-49 (1988).
27. Paczko, G., Lefdal, P. M., and Peters, N., *Twenty-First*

Symposium International on Combustion, The Combustion Institute, 1986, pp. 739-748.
28. Lindstedt, R. P., and Mauss, F. Paper presented at Third International Workshop on Asymptotic Methods and Reduced Chemistry, Cambridge, UK, July 1990.
29. Warnatz, J., *Eighteenth Symposium (International) on Combustion*, The Combustion Institute, 1981, p. 369.
30. Bockhorn, H., Moser, A., Wenz, H., and Warnatz, J., *Nineteenth Symposium (International) on Combustion*, The Combustion Institute, 1982, p. 197.
31. Warnatz, J., *Combust. Sci. Technol.* 34:177 (1983).
32. Frenklach, M., and Warnatz, J., *Combust. Sci. Technol.* 51:265 (1987).
33. Baulch, D. L., and co-workers, CEC Kinetics Data Evaluation Group, Summary (Provisional) of Preferred Rate Data for Combustion Modelling, September 1989.
34. Cernansky, N., Pitz, W., Wilk, R., and Westbrook, C., *Combust. Flame* 77:145 (1989).
35. Dagaut, P., Cathonnet, M., Boettner, J., and Gaillard, F., *Combust. Sci. Technol.* 56:23 (1987).
36. Lee, K. B., Thring, M. W., and Beer, J. M., *Combust. and Flame* 6:137 (1962).
37. Roper, F., Ph.D. thesis, University of Newcastle, 1979.
38. Nagle, J., and Strickland-Constable, R. F., *Proceedings of the Fifth Carbon Conference*, 1962, Vol. 1, pp. 1-62.
39. Garo, A., Lahaye, J., and Prado, G., *Twenty-First Symposium (International) on Combustion*, The Combustion Institute, 1986, pp. 1023-1031.
40. Garo, A., Prado, G., and Lahaye, J., *Combust. Flame* 79:226-233 (1990).
41. *JANAF Thermochemical Tables*, Dow Chemicals.
42. Tsuji, H., and Yamaoka, I., *Thirteenth Symposium (International) on Combustion*, The Combustion Institute, 1971, p. 723.
43. Puri, I. K., Seshadri, K., Smooke, M. D., and Keyes, D. E., *Combust. Sci. Technol.* 56:1 (1987).
44. Tsuji, H., and Yamaoka, I., *Twelfth Symposium (International) on Combustion*, The Combustion Institute, 1969, pp. 917.
45. Harris, S. J., *Combust. Sci. Technol.* 72:67-77 (1990).
46. Neoh, K., Howard, J. B., and Sarofirm, A. F., *Twentieth Symposium (International) on Combustion*, The Combustion Institute, 1984, p. 951.
47. Roth, P., Brandt, O., and von Gersum, S., Presented at the Twenty-Third Symposium (International) on Combustion, Orleans July 1990.
48. Kiefer, J. H., Al-Alami, M. Z., and Budach, K. A., *J. Phys. Chem.* 86:808-813 (1982).
49. Burcat, A., and Radhakrishan, K., *Combust. Flame* 60:157(1985).
50. Rao, V. S., and Skinner, G. B., *J. Phys. Chem.* 93: 1869-1876 (1989).
51. Tsang, W., *J. Phys. Chem. Ref. Data* 17:889 (1988).
52. Lindstedt, R. P., in preparation.
53. Harris, S. J., and Kennedy, I. M., *Combust. Flame* 78:390-397 (1989).

Received 5 October 1990; revised 30 July 1991